Screening Channel Competition in Core-Level X-ray Photoemission as a Probe of Changes in Ground-State Properties of Transition-Metal Compounds

Michel van Veenendaal
Dept. of Physics, Northern Illinois University,
De Kalb, Illinois 60115, and
Advanced Photon Source, Argonne National Laboratory,
9700 South Cass Avenue, Argonne, Illinois 60439

(Dated: June 29, 2006)

Core-level X-ray photoemission spectra for copper, manganese, and ruthenium compounds are calculated. A strong dependence of the spectral line shape on electron/hole doping, magnetic and orbital ordering is observed. The changes can be explained in terms of the competition between local and nonlocal screening effects. In contrast to earlier claims, we find that the changes do not result from additional quasiparticle states at the Fermi level but from a strong coupling of the different screening channels to changes in the ground state. The strong sensitivity of core-level XPS on the surrounding transition-metal atoms enables the study of temperature- and doping-induced changes in orbital occupation and ordering.

PACS numbers: 71.10.-w, 71.28.+d, 79.60.-i

I. INTRODUCTION

Recently, the use of hard X-rays has revived the interest in core-level X-ray photoemission spectroscopy (XPS) [1–4]. XPS with synchrotron radiation in the hard X-ray region has a probe depth of 60 Å. The spectral line shape therefore reflects much more the bulk properties than XPS with conventional laboratory X-ray sources. XPS measures the response of the valence electrons to the creation of a strong local potential resulting from the removal of a core electron and thus provides information on the screening dynamics of a material. The main line at low binding energy corresponds to configurations where additional charge is moved to the site with the core hole, thereby effectively screening the local potential [5, 6]. Often strong satellite features at higher binding energies are observed resulting from the large overlap between the ground state and unscreened final states. From the study of the relative intensities and energy positions of the main and satellite features, important information on strongly correlated systems has been obtained. Analysis of XPS has helped in the classification of materials as charge-transfer or Mott-Hubbard insulators [7] and the determination of important parameters, such as the on-site Coulomb interaction and the charge-transfer energy [5, 6]. For a deeper understanding of the spectral line shape, it is important to understand the effective range of the screening of the core-hole potential. Early interpretations were restricted to the Anderson impurity limit, thereby assuming that screening is mainly accomplished by electrons from ligands surrounding the metal site with the core-hole potential [5, 6]. By using larger clusters involving several metal sites, it was demonstrated [8, 9] that nonlocal screening effects involving neighboring metal sites contributed strongly. The presence of these nonlocal screening channels was clearly demonstrated by a study on $Ni_xMg_{1-x}O$ [10], where in the dilute limit (small x), the nonlocal screening channel is absent. Increasing the Ni concentration opens up nonlocal screening between different Ni ions. Recent papers [1–4] suggested the failure of this formalism in explaining high-resolution hard X-ray experiments on cuprates, manganites, and ruthenates and proposed the presence of additional quasiparticle states at the Fermi level [1–4] as those found in Dynamical Mean-Field calculations [11]. None of these papers explicitly showed a failure of the formalism of local and nonlocal screening. This paper demonstrates that nonlocal screening can explain the presence of low-binding energy features that are very sensitive to changes in the electronic surroundings due to temperature, doping, changes in orbital occupation and orbital/spin ordering. The outline of the paper is as follows. A general description of the Hamiltonian is given. We then discuss the following compounds in detail: the XPS line shape in cuprates and its dependence on hole and electron doping; XPS in manganites, where changes due to doping, temperature, and magnetic and orbital ordering are considered; ruthenates, where we study the effects of orbital ordering on the spectral line shape. We end with the conclusions.

II. HAMILTONIAN

Calculations are done using exact diagonalizations for small clusters. The total Hamiltonian is given by

$$H = \sum_{ij\alpha_1\alpha_2} t_{i\alpha_1,j\alpha_2} c^\dagger_{j\alpha_2} c_{i\alpha_1} + \sum_{i\alpha_1\cdots\alpha_4} U_{\alpha_1\alpha_2,\alpha_3\alpha_4} c^\dagger_{i\alpha_4} c^\dagger_{i\alpha_3} c_{i\alpha_2} c_{i\alpha_1}, \quad (1)$$

where $c^\dagger_{i\alpha}$ creates an electron on site i with orbital and spin degrees of freedom denoted by α. The first term

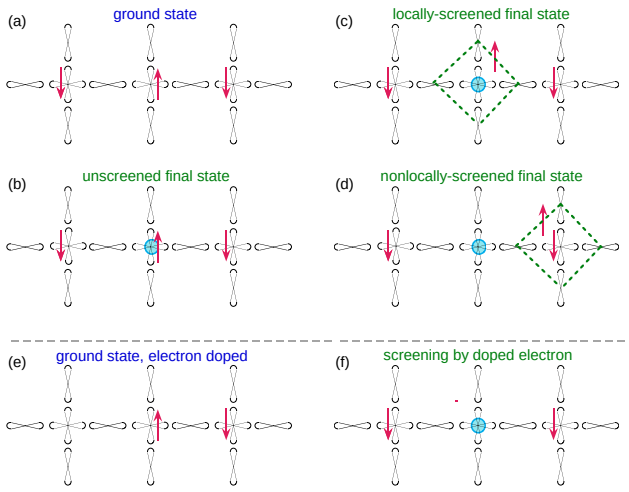

FIG. 1: (color online) (a) Schematic representation of the ground state in the undoped cuprates with on average one hole (indicated by the arrows) per CuO_4 plaquette. Shown are the $x^2 - y^2$ orbitals for the copper and the σ-bonding p orbitals of the oxygen. (b) Removal of a core electron leads to an XPS final state where the core hole (indicated by the blue circle) is unscreened. (c) Electrons can flow in from the oxygens surrounding the site with the core hole, thereby screening the core hole. This is known as local screening. (d) Screening electrons can come from neighboring CuO_4 plaquettes to screen the core hole. The state with two electrons is known as a Zhang-Rice singlet. (e) Schematic picture of the electron-doped system. (f) The lowest XPS final state where the doped electrons screen the strong core-hole potential.

on the right-hand side includes on-site energies ($i = j$) and nearest-neighbor hopping terms. The second term describes on-site Coulomb interactions. Core-level photoemission is generally well described by Fermi's Golden rule:

$$I(E_{\mathbf{k}}) = \sum_f |\langle f; E_{\mathbf{k}}|D|g; \hbar\omega\rangle|^2 \delta(E_g + \hbar\omega - E_f - E_{\mathbf{k}}),$$

where $|g\rangle$ and $|f\rangle$ are the ground and final states of the system, $\hbar\omega$ is the energy of the incoming photon, $E_{\mathbf{k}}$ is the kinetic energy of the outgoing photoelectron. In the case of hard X-rays, excitations are made into continuum states and the matrix element of the transition operator $D \sim \mathbf{p} \cdot \mathbf{A}$ causes a simple scaling of the isotropic spectrum. The spectral line shape is a result of the response of the valence system to the final-state local core-hole potential at a particular site $i = 0$, $H_c = -U_c \sum_\alpha c^\dagger_{0\alpha} c_{0\alpha}$. Core-hole valence-shell Coulomb multiplet effects are neglected. We now discuss how changes in charge, orbital and spin degrees of freedom change the core-level XPS spectra for several transition-metal compounds.

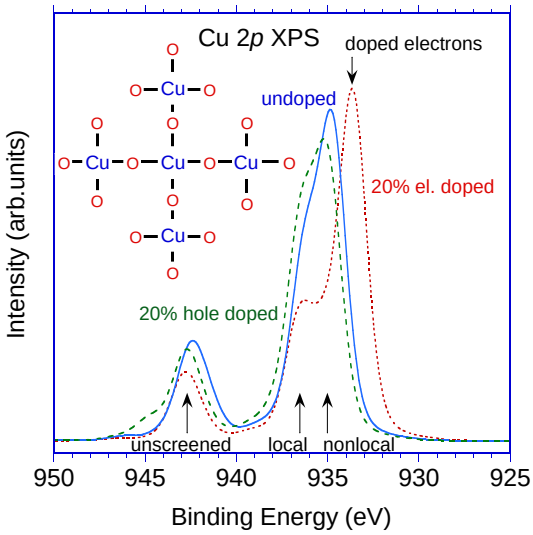

FIG. 2: (color online) Cu $2p$ XPS spectrum calculated for an undoped (blue solid), a 20% electron-doped (red dotted), and 20% hole-doped (green dashed) Cu_5O_{16} cluster.

III. CUPRATES

The presence of nonlocal screening effects was first demonstrated for copper oxides, such as CuO and the high-T_c superconductors [8, 9]. We follow here the approach as Refs. [8, 9] using exact diagonalization for a system with a reduced basis set of copper $x^2 - y^2$ and σ bonding oxygen $2p$ orbitals, see Fig. 1. We use a Cu_5O_{16} cluster (see the inset in Fig. 2). The parameters (for holes) are: a charge transfer $\Delta = 3.5$ eV, an oxygen band width $W_p = 1.3$ eV, a hopping term between copper and oxygen of $(pd\sigma) = 1.5$ eV, expressed in terms of Slater-Koster intergrals [12], an on-site dd Coulomb interacion $U_d = 8.8$ eV, and an core-hole potential U_c=6.0 eV.

Let us first consider the undoped system. In the ground state, there is on average one electron per CuO_4 plaquette, see Fig. 1(a), with approximately 70% copper and 30% oxygen character. The holes are coupled antiferromagnetically through a superexchange interaction. The removal of the $2p$ core electron leads to the creation of a strong local potential U_c on the copper site, see Fig. 1(b). This leads to a satellite feature of mainly $\underline{2p}3d^9$ character (where $\underline{2p}$ stands for a $2p$ hole) which is found at high binding energies (943 eV, see Fig. 2), due to the large repulsion between the core hole and the hole in the Cu $x^2 - y^2$ orbital. For lower final states, electrons come from the oxygen orbitals to the copper site and screen the core hole. Obviously, this cost an energy of the order of $\Delta - W_p$, however, this is easily overcome by the strong attraction between the core hole and the screening electrons. The screening electron can come from the oxygens surrounding the site with the core hole, see Fig. 1(c). This is known as a local screening

process and leads to final states of mainly $\underline{2p}3d^{10}\underline{L}$ character for the plaquette with the core hole, where $\underline{L}$ stands for a hole on the oxygen ligands. These final states are found around 936.5 eV, see Fig. 2. The lowest possible final states result from a nonlocal screening process [8, 9], where an electron from the ligands surrounding a neighboring CuO_4 plaquette screens the core-hole potential. This leads to a final state of mainly $\underline{2p}3d^{10}$ character, plus a Zhang-Rice singlet [13, 14] on a neighboring CuO_4 plaquette of mainly $3d^9\underline{L}$ character. This gives rise to the peak around 935 eV in the spectrum for the undoped (5 holes) Cu_5O_{16} cluster (blue solid line) in Fig. 2. The lower energy of the nonlocal screening states is related to the large stabilization energy of the Zhang-Rice singlet [13, 14], which are pushed out of the oxygen band in valence-band photoemission [14].

For 20% hole doping (6 holes, green dashed line), we see that the ratio of local and nonlocal screening changes, see Fig. 2 (note, that the spectra are normalized to the integrated intensity which remains unchanged upon electron or hole doping). The presence of Zhang-Rice singlets hinders the nonlocal screening process leading to a decrease in intensity at 935 eV. This is compensated by local screening processes at the high binding-energy side of the main line. For 20% electron doping, we see a large peak at 934 eV. This feature is clearly observed with XPS using hard X-rays [3, 4] whereas it is very weak for common laboratory soft X-ray sources. This clearly indicates the importance of hard X-rays in probing the bulk electronic structure. Upon electron doping, CuO_4 plaquettes with a $3d^{10}$ configuration are formed, see Fig. 1(e). The presence of additional electrons in the system allows screening of the core hole without involving the oxygen ligands, see Fig. 1. Therefore, the additional low binding-energy feature occurs at an energy equal to the charge-transfer energy below the main line in the undoped spectrum. Note that the intensity of the low-binding energy feature is much stronger than one would simply expect from a 20% electron-doped system. This indicates that there are strong dynamic effects. Taguchi *et al.* [3, 4] suggested that the low binding-energy feature is an indication of the presence of doping-induced states. However the spectra in Fig. 2 are obtained without changing the parameter set or introducing new states but simply by changing the number of valence electrons.

IV. MANGANITES

Manganites, such as $R_{1-x}A_xMnO_3$ (where R is a trivalent rare-earth ion and A is a divalent alkaline ion), have attracted attention due to the strong dependence of their conductance on magnetic field [15, 16], known as colossal magnetoresistance. They display a fascinatingly rich phase diagram due to the interplay between magnetism, local lattice distortions, and orbital ordering. The Mn $2p$ XPS was studied by Saitoh *et al.* [17]. Using exact diagonalization for a MnO_6 cluster, they concluded that, for $x = 0$, the main line has predominantly $\underline{2p}3d^5\underline{L}$ hole character. Due to the large hybridization for trivalent and tetravalent manganese compounds, the satellite of mainly $\underline{2p}3d^4$ character is very weak and about 10 eV higher in energy. Recently, using hard X-rays and a significantly better resolution, Horiba *et al.* [2] found a clear feature at low binding energy that showed a strong dependence on doping and temperature. They also used a MnO_6 cluster to interpret their data. However, in analogy to Dynamical Mean-Field Theory [11], which can be mapped onto a single-impurity Anderson model in infinite dimensions, they added states to represent a quasiparticle band at the Fermi level. Although agreement with the experimental line shape was obtained, this approach is unsatisfactory in several aspects. First, quasiparticle states at the Fermi level were needed to describe the spectral line shape for the undoped system ($x = 0$) [2], which is an insulator. The discrepancy was ascribed [2] to hole doping due to excess oxygen. Also, it is not obvious why additional quasiparticle states, as those found in Dynamical Mean-Field Theory [11] are necessary to explain the metallic behavior in the manganites. Metallic behavior occurs for doped systems, where the chemical potential shifts to the top of the lower Hubbard band. Secondly, the restriction to an Anderson impurity model removes the nonlocal screening channel that, as described above, can explain the additional features. In fact, the states at the Fermi level that were added in analogy Dynamical Mean-Field Theory mimic the nonlocal screening effect. Thirdly, new parameters for each doping level are necessary to describe the position of the states in the gap and the strength of the coupling of the manganese site with the quasiparticle states.

In describing Mn $2p$ XPS, we employ a Mn_8 cluster (see Fig. 4) with periodic boundary conditions thereby retaining the local cubic symmetry. In order to reduce the size of the calculation, we use a basis set of e_g type orbitals that effectively represent a MnO_6 cluster, see Fig. 3(a). This implies that the t_{2g} and oxygen states are projected out. The t_{2g}^3 core spins are treated classically in the framework of a double-exchange model [19]. The calculation of the effective parameters for this reduced basis set requires care. Effective parameters for ground (final) states were calculated using a MnO_6 including $(\underline{2p})3d^4$, $(\underline{2p})3d^5\underline{L}$, and $(\underline{2p})3d^6\underline{L}^2$ configurations with Coulomb parameters Racah $A = 5.36$, $B = 0.12$, and $C = 0.45$ eV [18], a cubic crystal-field of 1.5 eV, and a charge-transfer energy $\Delta = E_{\rm low}(3d^5\underline{L}) - E_{\rm low}(3d^4) = 1.8$ eV. The hybridization between the manganese and oxygen is given in terms of Slater-Koster parameters [12] $(pd\sigma) = -1.8$ and $(pd\pi) = 0.9$ eV. For the core-hole potential, we take $U_c = 6$ eV. It is important to realize that the parameters for the effective e_g orbitals are substantially different from the parameters for the $3d$ orbitals. The effective hopping $(dd\sigma)$ is -0.4 eV is reduced due to the hopping through the oxygens. The effective on-site repulsion is

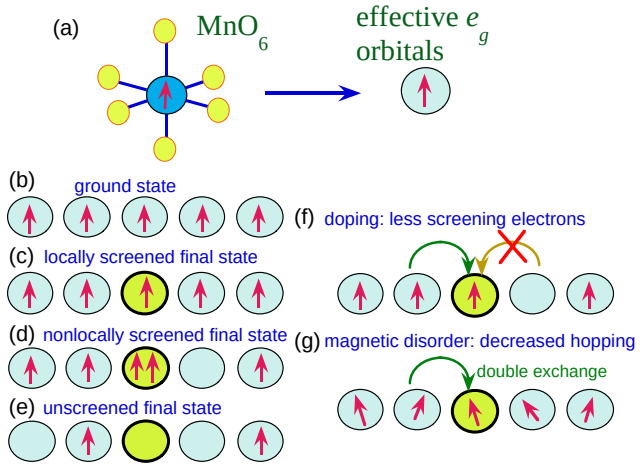

FIG. 3: (color online) (a) Calculations for the manganites are done for a reduced basis set, where effective e_g orbitals correspond to a MnO_6 unit. (b) Schematic picture of the ground state of the undoped system, where there is on average one e_g electron per site. (c) A locally screened final state, where the core hole (indicated by the thick green circle) is screened by electrons on the MnO_6 unit. (d) A nonlocally screened final state, where screening electrons come from neighboring MnO_6 units. (e) For doped systems, final states can be reached where there are no e_g electrons that screen the core hole. (f) Schematic picture of the reduction of the nonlocal screening channel for hole-doped manganites. Doping reduces the number of e_g electrons that could screen the core hole. (g) Reduction of the nonlocal screening channel due to magnetic disorder. When the core spin fluctuate, the double exchange mechanism hampers the hopping between different sites.

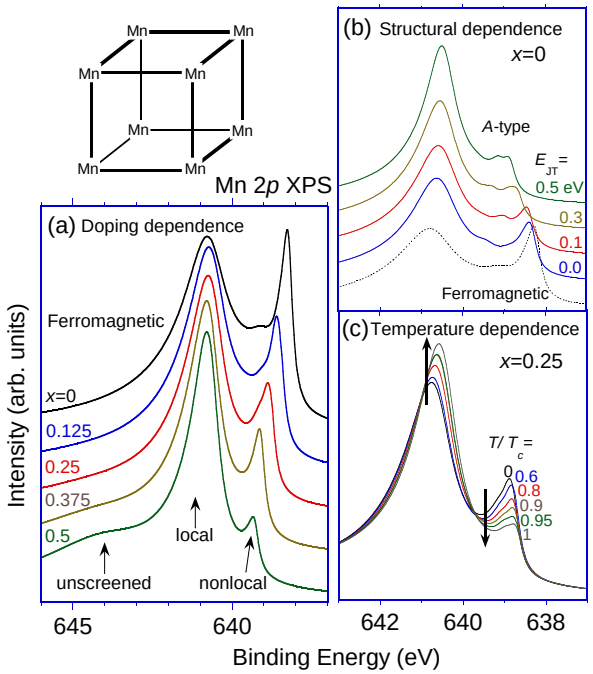

FIG. 4: (color online) Mn $2p$ XPS line shapes calculated for a Mn_8 cluster. (a) Doping dependence for $R_{1-x}A_xMnO_3$ with $x = 0, 0.125, 0.25, 0.375$, and 0.5 (coresponding to 8, 7, 6, 5, and 4 e_g electrons in the Mn_8 cluster). (b) Comparison of the Mn $2p$ XPS for $x = 0$ (8 e_g electrons) for different magnetic and orbital structures. The dotted and solid lines show the ferromagnetic and A type magnetic structures, respectively. $3x^2 - r^2/3y^2 - r^2$ orbital ordering is induced by a Jahn-Teller splitting between the $(y/x)^2 - z^2$ and $3(x/y)^2 - r^2$ orbitals of $E_{JT} = 0$ (no orbital ordering), 0.1, 0.3, and 0.5 eV. (c) Temperature dependence of the Mn $2p$ XPS for $x = 0.25$ (6 e_g electrons) for $T/T_c = 0, 0.6, 0.8, 0.9, 0.95$, and 1.

given by

$$U_{\rm eff} = E_{\rm low}(5) + E_{\rm low}(3) - 2E_{\rm low}(4), \qquad (2)$$

where $E_{\rm low}(n)$ is the lowest energy for the MnO_6 cluster with n electrons. The effective on site repulsion is then 1.7 eV. Note that this is significantly less that the $U_{\rm eff}$ for Mn ions, $A - 8B = 4.4$ eV. This is due to the fact that the transfer between different MnO_6 units is of the charge-transfer type, i.e. an electron is transferred from oxygen to manganese. Therefore, $U_{\rm eff}$ is of the order of the charge-transfer energy Δ. The effective core-hole potential is given by

$$U_{c,\rm eff} = E^c_{\rm low}(4) - E_{\rm low}(4), \qquad (3)$$

where $E^c_{\rm low}(n)$ is the lowest energy for the MnO_6 cluster with n electrons in the presence of a core-hole potential. The core-hole potential for the effective Mn e_g orbitals is 3.3 eV and strongly reduced with respect to the ionic U_c. This is a result of the reduction of the ionic U_c due to screening electrons from the oxygen ligands surrounding the manganese. Due to this local screening, the lowest configuration is $3d^5\underline{L}$ which is approximately $U_c - \Delta$ lower in energy.

Figure 4 shows the Mn $2p$ XPS spectrum for ferromagnetic ($T = 0$) $R_{1-x}A_xMnO_3$ for $x = 0, 0.125, 0.25, 0.375$, and 0.5, coresponding to 8, 7, 6, 5, and 4 e_g electrons in the Mn_8 cluster, respectively. The spectrum has a peak at 641 eV corresponding to the locally screened final state, where the effective MnO_6 unit has one e_g electron, see Fig. 3(d). Note, that the local screening is included by a reduction of the core-hole potential for the effective e_g orbital. At low binding energy, we see a peak that is strongly doping dependent. This corresponds to the nonlocal screening channel leading to a final state with two e_g electrons on the site with the core hole, see Fig. 3(d). The strength of the nonlocal screening strongly decreases with increasing hole doping reflecting the lower probability of creating a doubly-occupied (e_g^2) site with fewer e_g electrons in the system, see Fig. 3(f). For larger hole doping, unscreened final states are reached without e_g electrons on the site with the core hole, see Fig. 3(e), leading to an increase in intensity at 644 eV.

Although, experimental Mn $2p$ XPS [2] shows a decrease in intensity for the low binding-energy peak for $x > 0.2$, this feature is considerably weaker in the $x = 0$ spectrum, indicating that it is not only the electron density that affects the spectral weights. To account for that, we have to include the fact that $R\mathrm{MnO_3}$ has an A-type magnetic structure, i.e., ferromagnetic planes coupled antiferromagnetically. Within a double-exchange framework [19], the effective hopping is given by $\cos\frac{\theta_{ij}}{2}$, where θ_{ij} is the difference in angle between the t_{2g}^3 core spins on neighboring sites i and j. Therefore, for the A-type magnetic structure the nonlocal screening channel between antiferromagnetically coupled planes is strongly reduced leading to a decrease in spectral weight of the low binding-energy feature, see the blue line in Fig. 4(b) (indicated by $E_{\mathrm{JT}} = 0.0$). In addition, the undoped system shows orbital ordering with alternating $3x^2-r^2/3y^2-r^2$ orbitals. The orbital ordering is induced by a Jahn-Teller splitting between the $(y/x)^2-z^2$ and $3(x/y)^2-r^2$ orbitals of $E_{\mathrm{JT}} = 0$ (no orbital ordering), 0.1, 0.3, and 0.5 eV. Figure 4 shows that the nonlocal screening decreases for larger values of E_{JT}, indicating a sensitivity of core-level XPS for orbital ordering.

Changes in the relative efficiency of the local and nonlocal screening are also observed as a function of temperature. Figure 4 shows the Mn $2p$ XPS for ferromagnetic $R_{0.75}A_{0.25}\mathrm{MnO_3}$ for $T/T_c = 0, 0.6, 0.8, 0.9, 0.95$, and 1, where T_c is the critical temperature. Within the double-exchange model [19], the effective hopping depends on $\langle\cos\frac{\theta_{ij}}{2}\rangle$. For $S = 3/2$ spins, the hopping reduces by 5/8 for T/T_c is 0 to 1. The reduced hopping decreases the nonlocal screening effect with respect to the local screening, see Fig. 3(g), leading to a concomitant decrease in intensity of the low binding-energy feature. This agrees well with the experimental data [2]. This temperature dependence is a clear confirmation of the presence of double-exchange effects in manganites.

V. RUTHENATES

Recently, Kim *et al.* [1] proposed a new mechanism using dynamical mean-field theory [11] to interpret core-level XPS data on several ruthenium-based compounds. They ascribed the low binding-energy features to the presence of quasiparticle peak inside the gap. However, discrepancies exist between the change in the low binding-energy feature and the observed metal-insulator transition. For the pyrochlore system $\mathrm{Y_{2-x}Bi_xRu_2O_7}$, a metal-insulator transition between $x = 0$ and $x = 0.4$ was necessary to explain the changes in the XPS line shapes. However, transport properties [20] and valence-band photoemission [21] show the transition around $x = 0.9$. Furthermore, a change in U/W of about 75% is necessary to obtain the experimentally observed spectral weight of the XPS low binding-energy feature. This is surprising since the Ru-O-Ru bond angle changes only from 128° to 135° for $x = 0$ to 2. On the other hand, it has been

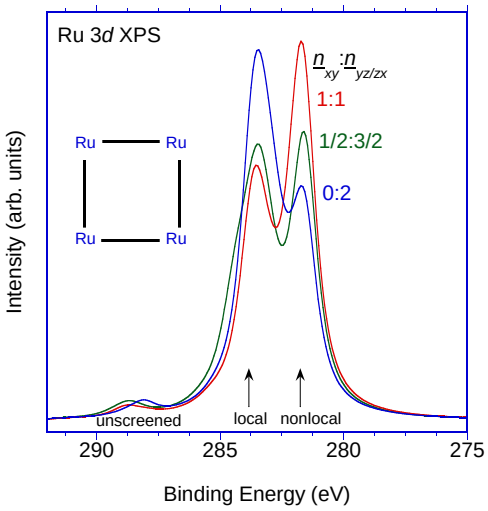

FIG. 5: (color online) Ru $3d$ XPS line shapes for a $\mathrm{Ru_4}$ cluster for different orbital occupations. The ratio between the $\underline{n}_{xy}$ and $\underline{n}_{yz/zx}$ holes is varied by introducing an energy difference ΔE between the xy and yz/zx orbitals. Spectra are given for $\underline{n}_{xy} : \underline{n}_{yz/zx} = 1 : 1, \frac{1}{2} : \frac{3}{2}$, and 0:2 for $\Delta E = 0.01, 0$, and -0.32 eV, respectively.

argued [22, 23] that, although correlation effects are important, the key to understanding the ruthenates lies in the competition between different orbital degrees of freedom. Mizokawa *et al.* [22] observed a strong temperature dependence in the t_{2g} occupations in $\mathrm{Ca_2RuO_4}$ resulting from the strong Ru $4d$ spin-orbit coupling combined with a small distortion of the $\mathrm{RuO_6}$ octahedra. Figure 5 shows that changes in orbital occupation drastically affect the Ru $3d$ XPS spectrum. For the calculation, a $\mathrm{Ru_4}$ cluster, see Fig. 5, with a reduced basis set of t_{2g} orbitals is used. Hopping integrals are $t_{xy} = 0.44$ and $t_{yz/zx} = 0.31$ eV [23], the on-site Coulomb terms are $U = 2$ and $U_c = 3$ eV. The number of t_{2g} electrons is four per Ru site. The ratio between the number of holes per site in the xy orbital $\underline{n}_{xy}$ and the yz/zx orbitals $\underline{n}_{yz/zx}$ is varied by an energy difference ΔE that stabilizes the xy orbitals with respect to the yz/zx orbitals. Figure 5 shows the Ru $3d$ XPS spectra for $\underline{n}_{xy} : \underline{n}_{yz/zx} = 1 : 1, \frac{1}{2} : \frac{3}{2}$, and 0:2 for $\Delta E = 0.01, 0$, and -0.32 eV, respectively. The finite cluster size makes the changes in hole occupations discrete. We observe a low binding-energy feature corresponding to the non-local screening process where an electron from a neighboring site is added to the site with the core hole to screen the strong core-hole potential. This screening process is much stronger for the planar xy orbitals due to the larger coupling with the neighboring $\mathrm{RuO_6}$ units in the plane. A decrease in the number of xy electrons that can be added to the site leads to a decrease in the nonlocal screening channel. Temperature-dependent hard X-ray photoemission experiments on $\mathrm{Ca_2RuO_4}$ would provide a test of the relationship between XPS and the $\underline{n}_{xy} : \underline{n}_{yz/zx}$ ratio [22].

VI. CONCLUSIONS

Core-level X-ray photoemission spectra have been calculated for copper, manganese, and ruthenium compounds. It has been shown that the strong changes in spectral line shape are a result of the competition between local and nonlocal screening channel and are most likely not indicative of the appearance of quasiparticle states at the Fermi level [1–4]. It also removes discrepancies between the XPS spectra and conductivity measurements for the manganites and the ruthenates. Experimentally, low-binding energy peaks are found for systems that are insulating. This is difficult to reconcile with an interpretation that ascribes these features to a quasiparticle band at the Fermi level.

The strong dependence of nonlocal screening on the electronic and magnetic surroundings make core-level XPS extremely suited to probe changes in local magnetic couplings, orbital occupations and orbital ordering. It would be interesting to study the XPS for manganites across a transition where charge or orbital ordering appears. For example for half-doped manganites, a CE type or undoped A type structures orbital ordering appears at a particular temperature. XPS might be helpful in distinguishing two different scenarios of orbital ordering: The orbital ordering temperature indicates the onset of the orbital ordering or at the orbital ordering temperature short-range orbital ordering, already present above the critical temperature, forms long-range order. Since XPS is sensitive to the local surroundings the first scenario would imply a sudden change in the XPS line shape, whereas in the second scenario the difference between XPS line shapes above and below the critical temperature would be small.

We thank Serkan Erdin and Ken Ahn for valuable discussions. This work was supported by the U.S. Department of Energy (DE-FG02-03ER46097) and the Institute for Nanoscience, Engineering, and Technology at Northern Illinois University under a grant from the U.S. Department of Education. Work at Argonne National Laboratory was supported by the U.S. Department of Energy, Office of Basic Energy Sciences, under contract W-31-109-Eng-38.

[1] H.-D. Kim, H.-J. Noh, K. H. Kim, and S.-J. Oh, Phys. Rev. Lett. **93**, 126404 (2004).
[2] K. Horiba, M. Taguchi, A. Chainani, Y. Takata, E. Ikenaga, D. Miwa, Y. Nishino, K. Tamasaku, M. Awaji, A. Takeuchi, M. Yabashi, H. Namatame, M. Taniguchi, H. Kumigashira, M. Oshima, M. Lippmaa, M. Kawasaki, H. Koinuma, K. Kobayashi, T. Ishikawa, and S. Shin, Phys. Rev. Lett. **93**, 236401 (2004).
[3] M. Taguchi, A. Chainani, K. Horiba, Y. Takata, M. Yabashi, K. Tamasaku, Y. Nishino, D. Miwa, T. Ishikawa, T. Takeuchi, K. Yamamoto, M. Matsunami, S. Shin, T. Yokoya, E. Ikenaga, K. Kobayashi, T. Mochiju, K. Hirata, J. Hori, K. Ishii, F. Nakamura, and T. Suzuki, Phys. Rev. Lett. **95**, 177002 (2005).
[4] M. Taguchi, A. Chainani, N. Kamakura, K. Horiba, Y. Takata, M. Yabashi, K. Tamasuka, Y. Nishino, D. Miwa, T. Ishikawa, S. Shin, E. Ikenaga, T. Yokoya, K. Kobayashi, T. Mochiku, K. Hirata, and K. Motoya, Phys. Rev. B **71**, 155102 (2005).
[5] G. van der Laan, C. Westra, C. Haas, and G. A. Sawatzky, Phys. Rev. B **23**, 4369 (1981); J. Zaanen, C. Westra, and G. A. Sawatzky, *ibid.* **33**, 8060 (1986).
[6] O. Gunnarsson and K. Schönhammer, Phys. Rev. Lett. **50**, 604 (1983).
[7] J. Zaanen, G. A. Sawatzky, and J. W. Allen, Phys. Rev. Lett. **55**, 418 (1985).
[8] M. A. van Veenendaal and G. A. Sawatzky, Phys. Rev. Lett. **70**, 2459 (1993).
[9] M. A. van Veenendaal, H. Eskes, and G. A. Sawatzky, Phys. Rev. B **47**, 11 462 (1993).
[10] S. Altieri, L. H. Tjeng, A. Tanaka, and G. A. Sawatzky, Phys. Rev. B **61**, 13403 (2000).
[11] For a review, see A. Georges, G. Kotliar, W. Krauth, and M. J. Rozenberg, Rev. Mod. Phys. **68**, 13 (1996).
[12] J. C. Slater and G. F. Koster, Phys. Rev. **94**, 1498 (1954).
[13] F. C. Zhang and T. M. Rice Phys. Rev. B **37**, R3759 (1988).
[14] H. Eskes and G. A. Sawatzky, Phys. Rev. Lett. **61**, 1415 (1988).
[15] G. H. Jonker and J. H. van Santen, Physica (Utrecht) **16**, 337 (1950).
[16] Y. Tomioka, A. Asamitsu, Y. Moritomo, H. Kuwahara, and Y. Tokura, Phys. Rev. Lett. **74**, 5108 (1995).
[17] T. Saitoh, A. E. Bocquet, T. Mizokawa, H. Namatame, A. Fujimori, M. Abbate, Y. Takeda, and M. Takano, Phys. Rev. B **51**, 13 942 (1995).
[18] J. S. Griffith, *The Theory of Transition-Metal Ions* (Cambridge University Press, Cambridge, 1961).
[19] C. Zener, Phys. Rev. B **82**, 403 (1951); P. W. Anderson and H. Hasegawa, Phys. Rev. **100**, 675 (1955); P.-G. de Gennes, Phys. Rev. **118**, 141 (1960).
[20] K.-S. Lee, D.-K. Seo, and M.-H. Whangbo, J. Solid State Chem. **131** 405 (1997).
[21] J. Park, K. H. Kim, H.-J. Noh, S. J. Oh, J.-H. Park, H.-J. Lin, and C.-T. Chen, Phys. Rev. B **69**, 165120 (2004).
[22] T. Mizokawa, L. H. Tjeng, G. A. Sawatzky, G. Ghiringhelli, O. Tjernberg, N. B. Brookes, H. Fukazawa, S. Nakatsuji, and Y. Maeno, Phys. Rev. Lett. **87**, 077202 (2001).
[23] A. Liebsch and A. Lichtenstein, Phys. Rev. Lett. **84**, 1591 (2000).